UNCLASSIFIED

AD

102522

Armed Services Technical Information Agency

Reproduced   by

DOCUMENT SERVICE CENTER
KNOTT BUILDING, DAYTON, 2, OHIO

UNCLASSIFIED

AD No. 102522

ASTIA FILE COPY

WADC TECHNICAL REPORT 55-249

PRELIMINARY MEASUREMENTS OF NONSTEADY VELOCITIES IN A SINGLE STAGE AXIAL-FLOW COMPRESSOR

HSUAN YEH

HARRY M. CRONER

DONALD E. ANDREWS

THE JOHNS HOPKINS UNIVERSITY

JUNE 1956

FC

WRIGHT AIR DEVELOPMENT CENTER

PRELIMINARY MEASUREMENTS OF NONSTEADY VELOCITIES IN A SINGLE STAGE AXIAL-FLOW COMPRESSOR

HSUAN YEH

HARRY M. CRONER

DONALD E. ANDREWS

THE JOHNS HOPKINS UNIVERSITY

JUNE 1956

WRIGHT AIR DEVELOPMENT CENTER
AIR RESEARCH AND DEVELOPMENT COMMAND
UNITED STATES AIR FORCE
WRIGHT-PATTERSON AIR FORCE BASE, OHIO

FOREWORD

This report was prepared in the Mechanical Engineering
Department of The Johns Hopkins University on Contract AF-
33(616)-152, under Project No. 3066, "Gas Turbine Technology,"
Task No. 70153, "Compressor Blading Systems of High-Deflection
Angle." The report covers the last phase of the contract work,
which was under the direction of Dr. H. Yeh. Previous phases of
this contract work, which were under the direction of Dr. G. Wis-
licenus, resulted in the preparation of WADC TR 55-348, "Three-
Dimensional Flow in Turbomachinery," Volumes I and II, by
Leroy Smith.

This contract work was administered by the Fluid Dynamics
Research Branch of the Aeronautical Research Laboratory,
Wright Air Development Center, with Mr. S. Hasinger acting as
Task Scientist.

WADC TR 55-249

ABSTRACT

Fluctuation intensities at selected stations in an axial-flow compressor stage were measured. These measurements recorded the total fluctuation which consists of both periodic and random (turbulence) parts. Through the investigation on the periodic part of the fluctuation, an estimate can be made on the turbulence intensity.

The intensity of the induced velocity due to the rotor at points in front of the rotor is analyzed. Also investigated is the fluctuation intensity due to the periodic presence of wakes behind the rotor. Such analytical considerations are found to be in substantial agreement with the measured data.

The wake behind blades is found to decay and spread in the same manner as the wake behind single airfoils except in the immediate neighborhood of the following blade row, at which place the decay is accelerated.

PUBLICATION REVIEW

This report has been reviewed and is approved.

FOR THE COMMANDER:

ALDRO LINGARD
Colonel, USAF
Chief, Aeronautical Research Laboratory
Directorate of Research

TABLE OF CONTENTS

LIST OF FIGURES

LIST OF FIGURES

1. Introduction

Recent interest on the investigation of nonsteady flows in an axial-flow turbomachine seems to be centered mostly on the phenomenon of stall propagation and surge. Results on this type of measurement have been reported by Huppert and Benser (Ref. 1), Iura and Rannie (Ref. 2), and Emmons, Pearson and Grant (Ref. 3). By comparison, few investigations on the nonsteady flows in the normal operating range of an axial-flow turbomachine have been reported. This is undoubtedly due to the general belief that as long as the machine is not in the stalling range, the nonsteady part of the flow due to turbulence and/or the relative motion between neighboring blade rows does not influence the performance of the machine to any great extent. Hence present day design is still based on the assumption of steadiness and often also of axial-symmetry, modified and refined if necessary by the consideration of (axially non-symmetrical) secondary flows. (Secondary flow in its commonly accepted sense is still a steady flow phenomenon relative to the blade passage.) A previous report by Smith (Ref. 4) issued in this laboratory under the same contract is one example of the effort along that direction.

It is inevitable, however, that as the art of the science advances, a deeper insight into the complicated flow phenomenon in an

---

NOTE: This report was released for publication in December 1955.

axial-flow turbomachine can be gained only through the additional

investigation of the non-steady part of the flow. Kemp and Sears

(Ref. 5) were the first ones to report on the influence on the overall

characteristics (such as lift, moment, and induced drag) of the blades

of a cascade due to the interaction between stationary and moving blade

rows. A different formulation on this problem by means of conformal

transformation was reported by Woods (Ref. 6). Recently in this

laboratory, Meyer (Ref. 7) made a detailed calculation on the nonsteady

parts of pressure and velocity distribution on a blade surface due to

the action of the travelling viscous wakes shed from an upstream cas-

cade of blades. This type of flow, although nonsteady, is still periodic.

On the other hand, there exists also the random type of nonsteady flow

or turbulence. It is to be expected that either type of fluctuations will

effect the profile drag (as distinct from the induced drag) and the

maximum attainable lift coefficient of the blades. Furthermore, in

at least one case the non-steady part of the flow may be decisive in

the normal performance of the machine. This is the case of com-

pressors with small blades operating at high altitudes so that Reynolds

number is low enough to be in the transition range. Whether the

boundary layer along the blades will be mostly laminar or mostly tur-

bulent or whether there will be laminar separation will presumably

depend on the nonsteady as well as the steady character of the flow.

This report presents a series of preliminary nonsteady velocity measurements in a single-stage experimental compressor with Reynolds number approximately 20,000 (based on blade chord length). Results include the intensity and the decay of wakes, the induced velocity upstream of the rotor and the turbulence level throughout the machine. Analysis was made insofar as possible to interpret the experimental results.

2. Testing Equipment

2-a. Compressor (Fig. 1). The low-speed single-stage compressor used in these experiments has been fully described in a previous report (Ref. 4). Briefly, the unit consists of a row of inlet guide vanes, followed by a rotor and a stator. It was designed so that the energy addition is proportional to the radius. The hub-tip diameter ratio is 0.5. A cross-sectional view of the unit indicating all the major dimensions is shown in Fig. 1.

One alteration on the unit has been made since the previous report. In order to investigate fully the decay and the spread of the wake behind the inlet guide vanes, the distance between the inlet guide vanes and the rotor has been increased by the addition of a spacer section of 5-1/16" in axial length. Fig. 1 shows this altered dimension.

2-b. <u>Traversing Apparatus</u> (Fig. 2). The holder for the conventional (static pressure, total pressure, 3-claw yaw, etc.) as well as the hot-wire probes is supported by two perpendicular sets of rails. The whole unit is designed in such a way that complete traversing of the probe can be made along axial, circumferential and radial directions. The probe can also be rotated about its own axis.

In order to make a detailed survey of the wake behind the inlet guide vanes, it is necessary to be able to insert the probe at a large number of stations behind the vanes in both tangential and axial directions. To avoid the drilling of a large number of holes in the casing, a portion (4" X 10") of the casing wall is replaced by a lattice of interchangeable sliding plexiglas blocks (Fig. 2). One of the blocks is provided with holes at desired locations through which a probe can be inserted. This "master" block can be shifted to any tangential and axial station and the entire lattice remains airtight. A circumferential survey at intervals of 1 degree can be easily made. This device proves to be so convenient that the authors would like to recommend it for future such surveys.

2-c. <u>Hot-wire Anemometer</u> (Fig. 3). To measure velocity fluctuations, a tungsten wire of .0002" diameter and about 1/16" long was used. The cold resistance of the wire was approximately 6 ohms,

and its time constant about 0.5 μ sec. The ratio of hot to cold re-sistance was fixed at 1.45.

The hot-wire anemometer equipment used in these experiments is of the constant-current type based on the design by Kovasznay (Ref. 8). The first stage of the amplifier has been modified to further reduce the noise level. A resistance-capacitance circuit is used for full compensation of the time lag of the wire. The compensating amplifier gives essentially flat response up to 10,000 cps. The noise level at the operating condition of these experiments is less than 0.1 mv at input. This corresponds to a turbulence intensity of much less than 0.001 (0.1%) in these measurements.

3. Description of Experiments

All measurements described in this report were made at one operating condition which was near the design point of the compressor and well to the right of the peak in the head-capacity curve. Hence the blades were not near stalling. For these preliminary measure-ments, the radial location of all probe points was arbitrarily fixed at 4-3/16" from the blade tip. This was roughly near the middle span of the blade.

The measuring stations along the axial direction were as follows (in the order of direction of flow):

Before inlet guide vanes - Station 1

Between inlet guide vanes and rotor - Stations 2, 3, 4, 5, 6

Between rotor and stator - Stations 7, 8

Between stator and exit - Stations 9, 10

The axial distances of these stations are shown in Fig. 1 and repeated

in Fig. 4. The latter figure is a cylindrical sectional view at the

measuring radius.

4. Results of Experiments

A detailed survey of the flow behind the inlet guide vanes was

made at Stations 2 to 6. The measurements included direction of

flow (by three-claw yaw probe), total pressure (by Kiel probe) and

static pressure (by spherical probe). Distributions of dynamic pressure

at various stations of the wake behind inlet guide vanes are shown in

Fig. 5.

The intensity of velocity fluctuation $\sqrt{\overline{u^2}}/\overline{U}$ (defined as the

ratio of the r.m.s. of the fluctuating velocity u to the mean

velocity $\overline{U}$) at all stations is as follows. (Unless stated otherwise,

the hot-wire is normal to the mean direction of flow.)

Location	Station	Case		Fluctuation Intensity $\sqrt{u^2}/U$ (%)
Before I. G. V.	1	1		0.24
Between I. G. V. and rotor	2	2a	in middle of wake	6.13
		2b	outside of wake	.39
	3	3a	in middle of wake	3.24
		3b	outside of wake	.35
	4	4a	in middle of wake	3.00
		4b	outside of wake	.30
	5	5a	in middle of wake	2.84
		5b	outside of wake	.45
	6	6a	in middle of wake	2.93
		6b	outside of wake	1.45
Between rotor and stator	7	7a	wire in tangential dir.	5.47
		7b	wire in axial dir.	2.20
	8	8	wire in tangential dir.	3.16
Behind stator	9	9	wire in tangential dir.	1.30
	10	10	wire in tangential dir.	1.32

Oscilloscope photographs of the instantaneous velocity for all cases (except Cases 4a and 4b) are reproduced in Fig. 6 to 11. The faint detached lines on top of the film strips are the images of a small neon bulb which flashes 120 times a second. These lines, therefore, fix the time scale of the abscissa. A sine wave of known voltage was fed into the amplifier (without compensation) and the image on the oscilloscope screen was photographed at the beginning of each

film strip. The voltage of the sine wave was adjusted in each case to give a picture of approximately the same height as that of the velocity fluctuations. All controls in the amplifier and the oscilloscope were left untouched between the taking of the sine wave and that of the instantaneous velocity. In this way the scale of the ordinate of the film strips is fixed in terms of input voltage of the amplifier. On the other hand, the relation between the voltage and the velocity fluctuations are established by the hot-wire. We therefore have a convenient means of estimating the magnitude of all instantaneous velocities.

5. Analysis and Interpretation

5a. Separation of Periodic and Random Fluctuations. Let the instantaneous velocity U be the sum of an average velocity $\bar{U}$ and a (total) fluctuating velocity u. The fluctuating velocity u in turn consists of periodic fluctuations u_p and random fluctuations u_r. (We here use the word "periodic" to describe the property of repeating from one rotor blade to another.) We have thus,

$$U(t) = \bar{U} + u_p(t) + u_r(t) \tag{1}$$

By definition

$$\bar{u}_p + \bar{u}_r = 0 \tag{2}$$

where a bar on top means time average. Eq. (2) indicates that $\overline{u}_p = -\overline{u}_r$ although $\overline{u}_p$ and $\overline{u}_r$ may not be zero individually. However, we can easily remove this complication by letting

$$u_p(t) = \overline{u}_p + u_p'(t)$$

$$u_r(t) = \overline{u}_r + u_r'(t)$$

(3)

Now $\qquad \overline{u_p'} = \overline{u_r'} = 0 \qquad$ by definition. (4)

Also $u_p + u_r = u_p' + u_r'$ by virtue of Eq. (2). The mean square of the total fluctuations becomes thus,

$$\overline{(u_p + u_r)^2} = \overline{(u_p' + u_r')^2} = \overline{u_p'^2} + \overline{u_r'^2} + 2\overline{u_p' u_r'}$$

Now since u_r' and u_p' are uncorrelated by definition, the last term $2\overline{u_p' u_r'}$ becomes $2\overline{u_p'}\,\overline{u_r'}$ (see for example Cramer, Ref. 9) which is zero on account of Eq. (4). Hence we have

$$\sqrt{\overline{u^2}} = \sqrt{\overline{(u_p + u_r)^2}} = \sqrt{\overline{u_p'^2}} + \sqrt{\overline{u_r'^2}}$$

(5)

Eq. (5) gives the intensity of total fluctuations in terms of the intensities of the individual periodic and random fluctuations. The experiment measures the first term, namely $\sqrt{\overline{u^2}}$. In order to make use of Eq. (5), we have to know in addition either $\overline{u_p'^2}$ or $\overline{u_r'^2}$. It is for this reason that the evaluations of $\overline{u_p'^2}$ before and after the rotor are presented in sections 5c and 5d.

5b. _Wake_. Fig. 5 shows the familiar phenomenon that the wake behind a body widens in the direction of flow while at the same time decreases its intensity. It is interesting to compare our case of wake behind inlet guide vanes with that behind a symmetrical two-dimensional body for which the following relations hold. (See Durand, Ref. 10, or Goldstein, Ref. 11.)

$$U_{d_{max}} \propto \frac{1}{x^{1/2}} \qquad\qquad (6)$$

$$y_0 \propto x^{1/2} \qquad\qquad (7)$$

where $U_{d_{max}}$ = maximum velocity defect in the wake.

y_0 = half-width of the wake, i.e., the distance between the center of the wake and its edge where $U = 0$.

and   x   = distance along direction of flow measured from a suitable origin.

The maximum velocity defect $U_{d max}$ in these experiments can be easily calculated from the dynamic pressure distribution. Fig. 12 shows a plot of $1/U_{d max}^2$ versus distance x ($U_{d max}$ is rendered non-dimensional as a ratio to the maximum velocity outside of the wake at Station 2). According to Eq. (6) this plot should be a straight line with the intercept on the abscissa at some distance

upstream of the trailing edge of the vanes. Fig. 12 shows that this is indeed true for a distance of about 2 chord lengths downstream of the guide vanes. The intercept of the straight line on the abscissa is at a distance of approximately 20% of chord length upstream of the trailing edge. This agrees well with the result on single airfoils by Silverstein, Katzoff and Bullivant (Ref. 12). However, after a distance of two chord lengths downstream the decay of the wake is greatly accelerated so that at Station 6 the value for $1/U_{d\,max}^2$ is considerably more than what it should be from the straight line relation. An obvious explanation is that the nonsteady induced velocity from the downstream rotor tends to increase the mixing of the non-uniform flow in the wake. The verification of this is the fact that such an induced velocity is found to be indeed appreciable at the same station. (See Section 5c.)

An attempt to plot wake width against distance to check Eq. (7) runs into the difficulty that the width is not well-defined. One could of course invent a representative width such as, for example, the ratio of the integrated area of the U_d (velocity defect) distribution curve to $U_{d\,max}$. However, such a procedure does not seem to be worthwhile when the distribution of dynamic pressure is not at all smooth as can be seen in Fig. 5. Nevertheless a rough check was made, and, according to expectation, it was again found that the rate of spread of wake follows Eq. (7) up to about two chord-lengths downstream, after that the rate of spread is accelerated.

The fluctuation intensity $\sqrt{\overline{u^2}}/U$ between the inlet guide vanes and the rotor is plotted against the axial distance in Fig. 13. The upper curve shows that the maximum turbulence intensity in the wake decreases with distance in the direction of flow. This result is similar to that reported by Townsend (Ref. 13, 14) for the wake behind a circular cylinder. Since Townsend's measurements started at a distance of 80 times cylinder diameter downstream of the cylinder whereas the last station (i.e., Station 6) in these measurements was only at a distance of 24 times maximum blade thickness from the trailing edge of the blades, no comparison between the two cases is possible.

The lower curve in Figure 13 shows that the fluctuation intensity outside of the wakes remains at a constantly low level for a distance of approximately two chord lengths behind the inlet guide vanes, after that the intensity increases rapidly due to the periodic, induced velocity of the downstream rotor. Examination of oscilloscope photographs shows that at Station 5 outside of wakes (Fig. 8, Case 5b) the nonsteady velocity begins to show signs of periodicity due to the passing of the rotor. At Station 6 (Fig. 9, Case 6b) the periodic velocity completely overwhelms the random velocity or turbulence. On the other hand, the nonsteady velocity in the wake at the same stations is still predominated by turbulence, since the amount of periodic velocity is much less than the amount of turbulence there.

The following section is an attempt to estimate the magnitude of the induced velocities such as the one shown in Fig. 9, Case 6b.

5c. <u>Induced Velocities due to a Moving Cascade.</u>   To analyze

the nonsteady velocities induced upstream due to the motion of a rotor

downstream, it is necessary to simplify the problem by considering

the rotor as a plane cascade of infinitely many blades or airfoils

bounded by two walls representing the casing and the hub (Fig. 14). We

shall, in this section, use the following notation (see Fig. 14):

x - direction along the span of the airfoils, or radial
direction in an axial-flow turbomachine.

y - direction of the "axis" of the cascade, or tangential
direction in an axial-flow turbomachine.

z - direction perpendicular to x and y, or axial
direction in an axial-flow turbomachine.

ξ - direction of the chord of the airfoils. The angle
between z and ξ is denoted by α .

η - direction perpendicular to ξ , in the y-z plane.

u, v, w - induced velocity components along x, y, z
respectively.

q_η - induced velocity along η .

Considering one airfoil of the cascade (Fig. 15), its action can

be approximated by a series of vortex lines (bound vortices) whose

circulation Υ is in general a variable along both the chord and the

span of the blade. Thus

$$\Upsilon = \Upsilon \, (\, \xi \, , \, x \,)$$

Because the circulation varies along the vortex line, trailing

vortices will be shed. According to Helmholtz' Law, the strength

of the trailing vortices is equal to $\frac{\partial \gamma}{\partial x}$. For first approxima-

tion, it is assumed that the trailing vortices move downstream

with the main velocity which, for cascades of thin airfoils, has

the direction of ξ . Since γ varies continuously along x

for a bound vortex line stationed at $\xi = \xi$, the resulting

trailing vortex lines will smear over the entire ξ -x plane,

from $\xi = \xi$ to $\xi = \infty$. The same holds true for all

other bound vortices. Finally, the blade is bounded by an upper

and a lower wall (casing and hub) whose action is identical to having

the same vortex pattern repeated as images to the two walls. Thus,

if L is the blade length, we must have

$$\gamma(-x) = \gamma(x) \qquad \gamma(L+x) = \gamma(L-x)$$

This is achieved by expressing γ in a Fourier cosine series,

$$\gamma(\xi, x) = \sum_{n=0}^{\infty} A_n(\xi) \cos \frac{n \pi x}{L} \qquad (8)$$

(1) <u>Bound Vortices.</u> Consider the induced velocity at any

upstream point P $(x_0, -y_0, -z_0)$ in the flow field due to a single

bound vortex line extending from x = -o to x = +o and located at

y = y, z = z (Fig. 16). The induced velocities along y- and z-

directions due to such a single vortex line are:

$$v = \int_{-\infty}^{+\infty} \frac{\gamma(x, \xi)(z_o + \xi \cos\alpha)\, dx}{4\pi\left[(y_o + \xi \sin\alpha)^2 + (z_o + \xi \cos\alpha)^2 + (x - x_o)^2\right]^{3/2}}$$

$$w = \int_{-\infty}^{+\infty} \frac{\gamma(x, \xi)(y_o + \xi \sin\alpha)\, dx}{4\pi\left[(y_o + \xi \sin\alpha)^2 + (z_o + \xi \cos\alpha)^2 + (x - x_o)^2\right]^{3/2}}$$

Integrating through the entire chord from $\xi = 0$ to $\xi = c$ (see Fig. 16) and summing up all blades in the cascade, we obtain the induced velocities due to all the bound vortices representing the infinite cascade:

$$v = \sum_{n=0}^{\infty} \int_0^c \int_{-\infty}^{+\infty} \frac{\gamma(x, \xi)(z_o + \xi \cos\alpha)\, dx\, d\xi}{4\pi\left[(y_o + \xi \sin\alpha \pm ns)^2 + (z_o + \xi \cos\alpha)^2 + (x - x_o)^2\right]^{3/2}}$$

$$w = \sum_{n=0}^{\infty} \int_0^c \int_{-\infty}^{+\infty} \frac{\gamma(x, \xi)(y_o + \xi \sin\alpha \pm ns)\, dx\, d\xi}{4\pi\left[(y_o + \xi \sin\alpha \pm ns)^2 + (z_o + \xi \cos\alpha)^2 + (x - x_o)^2\right]^{3/2}} \tag{9}$$

The evaluation of the above integrals in the general case will be quite difficult. It can be seen from Eq. (8) for $\gamma(x, \xi)$ that the computation would be facilitated if one had a table of the following definite integral:

$$I(a, x_o) = \int_{-\infty}^{+\infty} \frac{\cos x\, dx}{\left[a^2 + (x - x_o)^2\right]^{3/2}}$$

Such a table, however, does not seem to be available.

We consider next the following special case. If $\gamma = \gamma(\xi)$ only, Eqs. (9) then become

$$v = \sum_{n=0}^{\infty} \int_0^c \frac{\gamma(\xi)(z_0 + \xi \cos \alpha)\, d\xi}{2\pi\left[(y_0 + \xi \sin \alpha \pm ns)^2 + (z_0 + \xi \cos \alpha)^2\right]}$$

$$w = \sum_{n=0}^{\infty} \int_0^c \frac{\gamma(\xi)(y_0 + \xi \sin \alpha \pm ns)\, d\xi}{2\pi\left[(y_0 + \xi \sin \alpha \pm ns)^2 + (z_0 + \xi \cos \alpha)^2\right]} \qquad (10)$$

To reduce the above equations, one makes use of the fact that v and -w are the real and the imaginary parts of the following function,

$$v - iw = \sum_{n=0}^{\infty} \int_0^c \frac{\gamma(\xi)\, d\xi}{2\pi\left[i(y_0 + \xi \sin \alpha \pm ns) + (z_0 + \xi \cos \alpha)\right]}$$

This equation can obviously be obtained also by considering the complex potential of two-dimensional vortices to which the problem is now reduced.

From the relation

$$\coth(x + iy) = \sum_{n=-\infty}^{+\infty} \frac{1}{x + i(y - n\pi)}$$

we can write

$$\sum_{n=0}^{\infty} \frac{1}{(z_0 + \xi \cos \alpha) + i(y_0 + \xi \sin \alpha \pm ns)}$$

$$= \frac{\pi}{s} \coth \frac{\pi}{s}\left(z_0 + iy_0 + \xi e^{i\alpha}\right)$$

Hence,

$$v - i w = \frac{1}{2S} \int_0^c \coth \frac{\pi}{S} \left(z_0 + i y_0 + \xi e^{i\alpha} \right) \gamma(\xi) \, d\xi \tag{11}$$

We can now separate the real and imaginary parts, since

$$\coth(x + iy) = \frac{\tanh x \, \sec^2 y - i \tan y \, \operatorname{sech} x^2}{\tanh^2 x + \tan^2 y}$$

we have

$$v = \frac{1}{2S} \int_0^c \frac{\tanh \frac{\pi}{S} (z_0 + \xi \cos\alpha) \sec^2 \frac{\pi}{S} (y_0 + \xi \sin\alpha)}{\tanh^2 \frac{\pi}{S} (z_0 + \xi \cos\alpha) + \tan^2 \frac{\pi}{S} (y_0 + \xi \sin\alpha)} \gamma(\xi) \, d\xi$$

$$\tag{12}$$

$$w = \frac{1}{2S} \int_0^c \frac{\tan \frac{\pi}{S} (y_0 + \xi \sin\alpha) \operatorname{sech}^2 \frac{\pi}{S} (z_0 + \xi \cos\alpha)}{\tanh^2 \frac{\pi}{S} (z_0 + \xi \cos\alpha) + \tan^2 \frac{\pi}{S} (y_0 + \xi \sin\alpha)} \gamma(\xi) \, d\xi$$

For the special case of γ = const. from $\xi = 0$ to $\xi = c$ (rectangular loading), Eq. (11) can be integrated as follows,

$$v - i w = \frac{\gamma}{2\pi} e^{-i\alpha} \log_e \left[\frac{\sinh \frac{\pi}{S} (z_0 + i y_0 + c e^{i\alpha})}{\sinh \frac{\pi}{S} (z_0 + i y_0)} \right] \tag{13}$$

The evaluation of the above expression for a given cascade configuration (i. e., a given s, c, and α) is fairly straightforward.

To roughly estimate the induced velocities in the present investigation, we use an even simpler approximation of representing the blade by a single vortex line of strength Γ , located say at

$\xi = 0$. For this case,

$$v - i\,w = \frac{\Gamma}{2S} \coth \frac{\pi}{S}\left(Z_0 + i\,y_0\right) \tag{14}$$

the induced velocities v and w are plotted against y_0/s for various

values of Z_0/s (Fig. 17):

In the present investigation, at the measuring radius,

$$\frac{\Gamma}{S} = 1.52\ V_a$$

where V_a is the mean axial velocity. Also, c/s, or the ratio of

chord to spacing, for the rotor is 1.27. If one assumes, for example,

that the equivalent single vortex is located at the middle of the blade,

a simple calculation based on the geometry of the rotor (Fig. 4) shows

that measuring Station 6 is at a distance $Z_0/s = 0.8$ from the

vortex. Fig. 17 gives

$$\left(\frac{v}{\Gamma/2S}\right)_{max} \approx \left(\frac{w}{\Gamma/2S}\right)_{max} \approx 1.4\ \%$$

or,

$$\left(\frac{v}{V_a}\right)_{max} \approx \left(\frac{w}{V_a}\right)_{max} \approx 1.06\ \%$$

or,

$$\frac{\sqrt{\overline{v^2}}}{V_a} \approx \frac{\overline{w^2}}{V_a} \approx 0.75\ \%\ \ ^{*}$$

---

    * For sinusoidal functions, the r.m.s. value to the peak
value is $1/\sqrt{2}$. The variation of v and w with y_0/s is, how-
ever, not sinusoidal, although not far off from it.

The measured value of fluctuation intensity at Station 6 is 1.45%. Let us assume that the turbulence intensity is the same as its value at Station 4, namely .30%. Then the fluctuation intensity due to the induced velocities alone would be

$$\sqrt{\overline{u_p^2}}/\overline{U} = \sqrt{1.45^2 - .30^2} = 1.42 \ \%$$

according to Eq. (5). This figure would put the equivalent single vortex at approximately 40% of chord length from the blade leading edge. This is an entirely convincing figure. Furthermore, this figure also checks the fluctuation intensity at Station 5. (A more refined calculation is to use Eq. (12) or (13).)

If this analysis on induced velocities is correct (both fluctuation intensity measurements and oscilloscope photographs seem to attest to its validity), then the intensity of the nonsteady induced velocities can easily exceed 10% of mean velocity near the rotor blade (see Fig. 17). This would have the tendency to accelerate the decay and at the same time increase the width of the wakes. In the recent investigations by Sears and Kemp (Ref. 15) and Meyer (Ref. 7) on the influence of wakes in a turbomachine, the wake width was taken from measurements on single airfoils (Ref. 12) and therefore was assumed to be narrow compared to the chord. It appears that the results thus obtained may be somewhat exaggerated--the actual wake influence, thanks to the induced velocities, is probably less severe.

(2) <u>Trailing Vortices.</u>   When the blade vortex strength varies along the span, the trailing vortices shed from the blades produce an induced velocity in addition to that produced by the bound vortices discussed previously.

Using the notation of Figures 14 and 16, we investigate the velocity at P induced by the trailing vortex situated at x = x and along the direction of ξ , from $\xi = \xi$ to $\xi = \infty$. Let us express the location of P in the x, ξ, η coordinates system, i.e., P $(x_0, -\xi_0, -\eta_0)$.

The induced velocity at P due to one trailing vortex behind one blade (the reference blade) is:

$$ dq = \frac{1}{4\pi} \frac{\partial \gamma}{\partial x} \frac{1}{\sqrt{(x-x_0)^2 + \eta_0^2}} \left\{ 1 + \frac{\xi_0 + \xi}{\sqrt{(x-x_0)^2 + \eta_0^2 + (\xi + \xi_0)^2}} \right\} $$

This velocity can be resolved into its components, du along x and dq_η along η .

$$ du = \frac{1}{4\pi} \frac{\partial \gamma}{\partial x} \frac{\eta_0}{(x-x_0)^2 + \eta_0^2} \left\{ 1 + \frac{\xi_0 + \xi}{\sqrt{(x-x_0)^2 + \eta_0^2 + (\xi + \xi_0)^2}} \right\} $$

$$ dq_\eta = \frac{1}{4\pi} \frac{\partial \gamma}{\partial x} \frac{(x-x_0)}{(x-x_0)^2 + \eta_0^2} \left\{ 1 + \frac{\xi_0 + \xi}{\sqrt{(x-x_0)^2 + \eta_0^2 + (\xi + \xi_0)^2}} \right\} $$

Integrating the above expressions along x and along ξ , and summing up for all blades, we obtain the induced velocity due to all trailing vortices.

$$u = \frac{1}{4\pi} \sum_{n=-\infty}^{n=+\infty} \int_{-\infty}^{+\infty} \int_{0}^{c} \frac{\partial \gamma}{\partial x} \frac{(\eta_0 + ns\cos\alpha)}{(x-x_0)^2 + (\eta_0 + ns\cos\alpha)^2}$$

$$\left\{ 1 + \frac{\zeta_0 + \zeta + ns\cos\alpha}{\sqrt{(x-x_0)^2 + (\eta_0 + ns\cos\alpha)^2 + (\zeta + \zeta_0 + ns\sin\alpha)^2}} \right\} d\zeta \, dx \quad (15)$$

$$q_\eta = \frac{1}{4\pi} \sum_{n=-\infty}^{+\infty} \int_{-\infty}^{+\infty} \int_{0}^{c} \frac{\partial \gamma}{\partial x} \frac{(x - x_0)}{(x-x_0)^2 + (\eta_0 + ns\cos\alpha)^2}$$

$$\left\{ 1 + \frac{\zeta_0 + \zeta + ns\sin\alpha}{\sqrt{(x-x_0)^2 + (\eta_0 + ns\cos\alpha)^2 + (\zeta + \zeta_0 + ns\sin\alpha)^2}} \right\} d\zeta \, dx$$

Referring to x, y, z coordinates, the components v, w of the induced velocity are related to q_η in the following way.

$$v = q_\eta \cos\alpha$$

$$w = q_\eta \sin\alpha$$

These velocities v and w are to be added to the values given by Eqs. (9).

Solutions to the above equations have to be worked out numerically for each design.

It should be mentioned that in analyzing the induced velocities due to the rotor, only the influence of the steady part of the bound and trailing vortices of the rotor blades has been considered. The unsteady part of the bound and trailing vortices (caused by the inter-action of the stator) is assumed to be of smaller order of magnitude when compared to the steady part, and hence can be neglected.

5d. <u>Fluctuation Intensity Behind a Rotor</u>. To estimate the intensity of the periodic fluctuations caused by viscous wakes behind a rotor, it is interesting to perform the following simple analysis:

Let the velocity outside of the wakes be unity, and the velocity inside of the wakes be m. Therefore, m is a number between 0 and 1, depending on the distance downstream from the rotor. The smaller this distance, the smaller is m. Let $\mathcal{E}$ be the ratio of the width of the wake to the spacing between two blades (Fig. 18). It can be easily shown that the average velocity is $1 - (1 - m)\mathcal{E}$, and the r. m. s. of the fluctuation is $(1 - m) \sqrt{\mathcal{E}(1 - \mathcal{E})}$. The intensity of these periodic fluctuations (as a ratio to the average velocity) is therefore

$$\frac{\sqrt{\overline{u^2}}}{\overline{U}} = \frac{\sqrt{\mathcal{E}(1-\mathcal{E})}}{\left(\frac{1}{1-m}\right) - \mathcal{E}} \tag{16}$$

The peak fluctuation (in the wake measured from the mean) is, again as a ratio to the average velocity,

$$\frac{u_{max}}{\overline{U}} = \frac{1 - \mathcal{E}}{\left(\frac{1}{1-m}\right) - \mathcal{E}} \tag{17}$$

Fig. 19 shows Eq. (16) plotted for the fluctuation intensity in terms of m and $\mathcal{E}$. A close look at the condition of axial velocity fluctuation at the measuring Station 7 (see Fig. 10, Case 7a) shows that,*

---

* Since a hot-wire is sensitive only to the velocity component perpendicular to it, in the following u and U will be axial components for Case 7a and tangential components for Case 7b.

$$\varepsilon \approx .08 , \qquad u_{max}/\bar{U} \approx 18.2$$

This gives, from Eqs. (16) and (17)

$$m \approx 0.8 \qquad \sqrt{\overline{u_p^2}}/\bar{U} \approx 5.5 \text{ %}$$

This checks closely the measured value of fluctuation intensity of

5.47%. The contribution of turbulence to the total fluctuation in-

tensity is probably small.

$$* \ * \ * \ * \ * \ * \ * \ * \ * \ * \ * \ *$$

We now turn our attention to Case 7b, namely the tangential

velocity fluctuations behind the rotor. A simple analysis based on the

assumption that the exit velocity always maintains a constant direc-

tion relative to the blade (although the magnitude of the relative

velocity decreases in the wake) gives immediately the ratio m' of

the tangential velocity in the wake to the tangential velocity outside

the wake as a function of m for the axial velocity and the blade

geometry. Referring to Fig. 20, it can be seen that

$$m' = \frac{(1-m) V_a \tan\alpha + V_u}{V_\theta} = 1 + (1-m)\left(\frac{V_u}{V_\theta} - 1\right)$$

where, following convention, V_u = blade velocity, V_θ = absolute

tangential velocity, and V_a = axial velocity.

For the case under consideration, $V_u/V_\theta = \frac{1}{.765}$, $m = 0.80$, then $m' = 1.0616$. Eqs. (16) and (17) can again be applied with m' instead of m. It is found that the intensity of periodic fluctuation due to wakes is

$$\sqrt{\overline{u_p^2}}/\overline{U} = 1.7\%$$

The measured total fluctuation intensity is 2.2%. From Eq. (5), the turbulence intensity can be estimated,

$$\sqrt{\overline{u_r^2}}/\overline{U} = \sqrt{2.2^2 - 1.7^2} = 1.4\%$$

An examination of Fig. 10, Case 7b, shows that the turbulence level indeed appears to be of the same order of magnitude as the periodic wakes.

It might be added that although the accuracy of constant-current type of hot-wire anemometer is presumably in doubt for very large fluctuations, the value of $u'_{max}/U = 18\%$ obtained in the wake of rotor blades checks very well with the wake survey behind inlet guide vanes at comparable distance from the blades.

References

1. Huppert, M. C., and Benser, W. A.: "Some Stall and Surge
    Phenomena in Axial-Flow Compressors," Journal of the
    Aeronautical Sciences, December, 1953.

2. Iura, T., and Rannie, W. D.: "Observations of Propagating
    Stall in Axial-Flow Compressors," Report No. 4, Me-
    chanical Engineering Laboratory, California Institute of
    Technology, April, 1953.

3. Emmons, H. W., Pearson, C. E., and Grant, H. P.:
    "Compressor Surge and Stall Propagation," Paper No.
    53-A-65, Presented at the Annual Meeting of A. S. M. E.,
    November-December, 1953.

4. Smith, L. H.: "Three-Dimensional Flow in Axial Flow
    Turbomachinery," Part I, "Theoretical Determination
    of Secondary Flow," Part II, "Experimental Investiga-
    tions," Submitted to Wright Patterson Air Force Base,
    Contract AF 33-(616)-152. Internal Flow Research
    Report I-14, Mechanical Engineering Department, The
    Johns Hopkins University, May, 1954. WADC TR 55-348, Volume I

5. Kemp, N. H., and Sears, W. R.: "Aerodynamic Interference
    between Moving Blade Rows," Journal of Aeronautical
    Sciences, September, 1953.

6. Woods, L. C.: "On Unsteady Flow through a Cascade of
    Aerofoils," Proceedings of Royal Society, Series A,
    February 15, 1955, pp. 50-65.

7. Meyer, R. X.: "Interference due to Viscous Wakes between
    Stationary and Rotating Blades in Turbomachines."
    Submitted to Office of Naval Research, Contract
    Nonr 248(45). Internal Flow Research Report I-24,
    Mechanical Engineering Department, The Johns Hopkins
    University, May, 1955.

8. Kovasznay, L. S. G.: "Development of Turbulence Measuring
    Equipment," NACA TN 2839, January, 1953.

9. Cramer, H.: "Mathematical Methods of Statistics,"
    Princeton University Press, 1946, p. 173.

10. Durand, W. F.: "Aerodynamic Theory," Vol. III, p. 165, 166.

11. Goldstein, S.: "Modern Developments in Fluid Dynamics,"
    Vol. II, p. 581-584. Clarendon Press, 1938.

12. Silverstein, A., Katzoff, S., and Bullivant, W. K.: "Downwash
    and Wake Behind Plain and Flapped Airfoils," NACA TR 651,
    1938.

13. Townsend, A.A.; "Measurements in the Turbulent Wake of a
    Cylinder," Proceedings of Royal Society, A190, 1947.

14. Townsend, A.A.: "Momentum and Energy Diffusion in the
    Turbulent Wake of a Cylinder," Proceedings of Royal
    Society, A197, 1949.

15. Sears, W. R.: Some Aerodynamic Problems of Compressors
    and Turbines, U. of Maryland Inst. for Fluid Dynamics
    Lecture Series No. 30, 1953.

    Kemp, N. H.: Nonsteady Aerodynamic Effects in Axial-Flow
    Turbomachines, Ph.D. Thesis, Cornell U., June 1953.

43 Blades Inlet Guide Vanes I.G.V.
21 " Rotor R.
25 " Stator S.

39 13/32"

Survey Stations

Survey Radius

22 5/32"

16 1/2"

14 1/32"

S.

R.

5 1/2" 5 1/16" 5" 5 31/32" 3 7/8"

4" 3" 5 1/16" 4 1/2"

6 1/2" 6" 6" 6 3/16" 5 7/8"

I.G.V.

6 3/16"

Cloth Intake Enclosure

18 3/4"

29 1/2"

Figure I. Cross Section of Testing Compressor
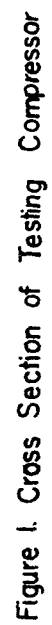
Figure 2 Traversing Apparatus
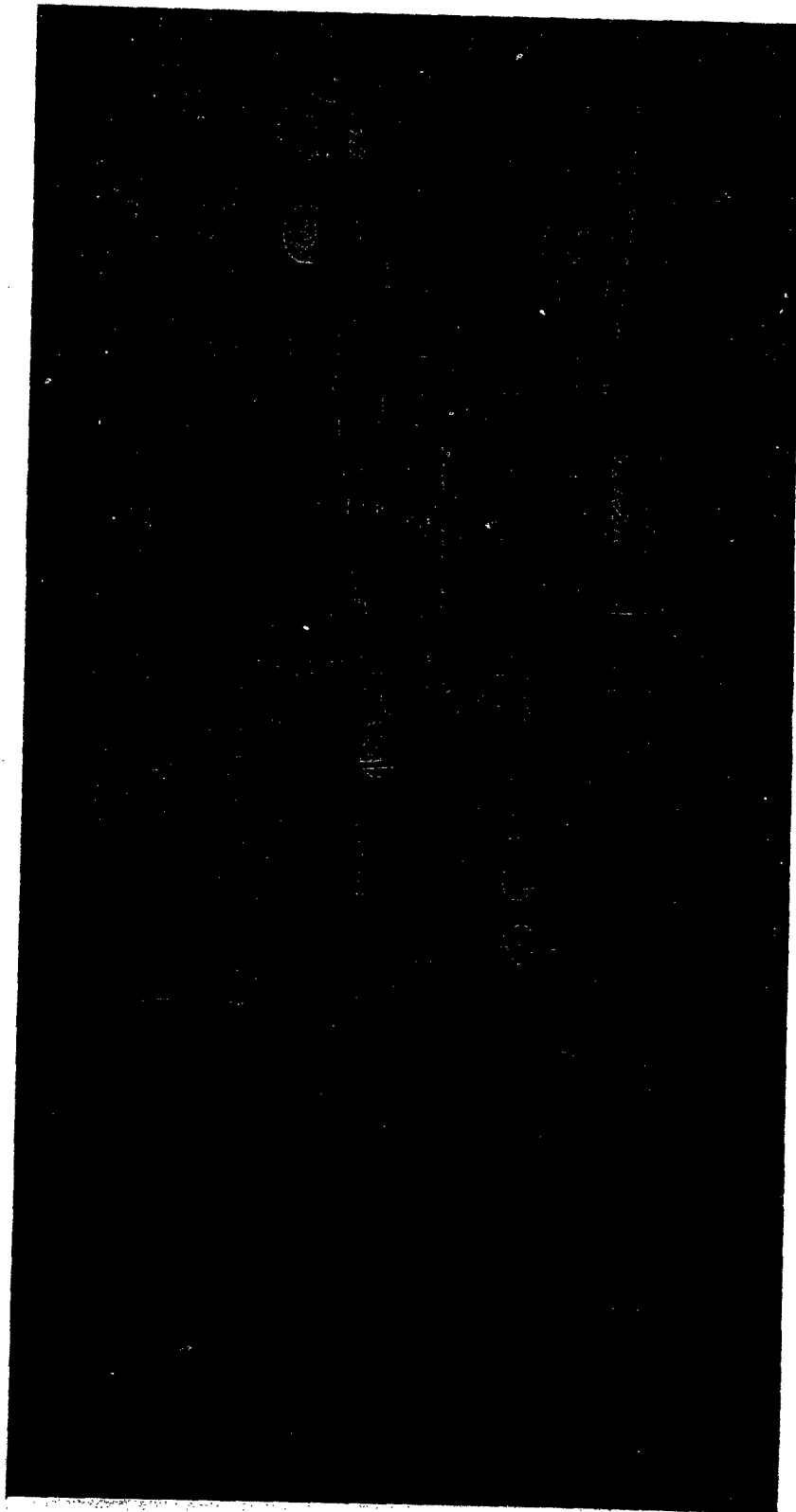
Figure 3 Hot-Wire Anemometer Equipment
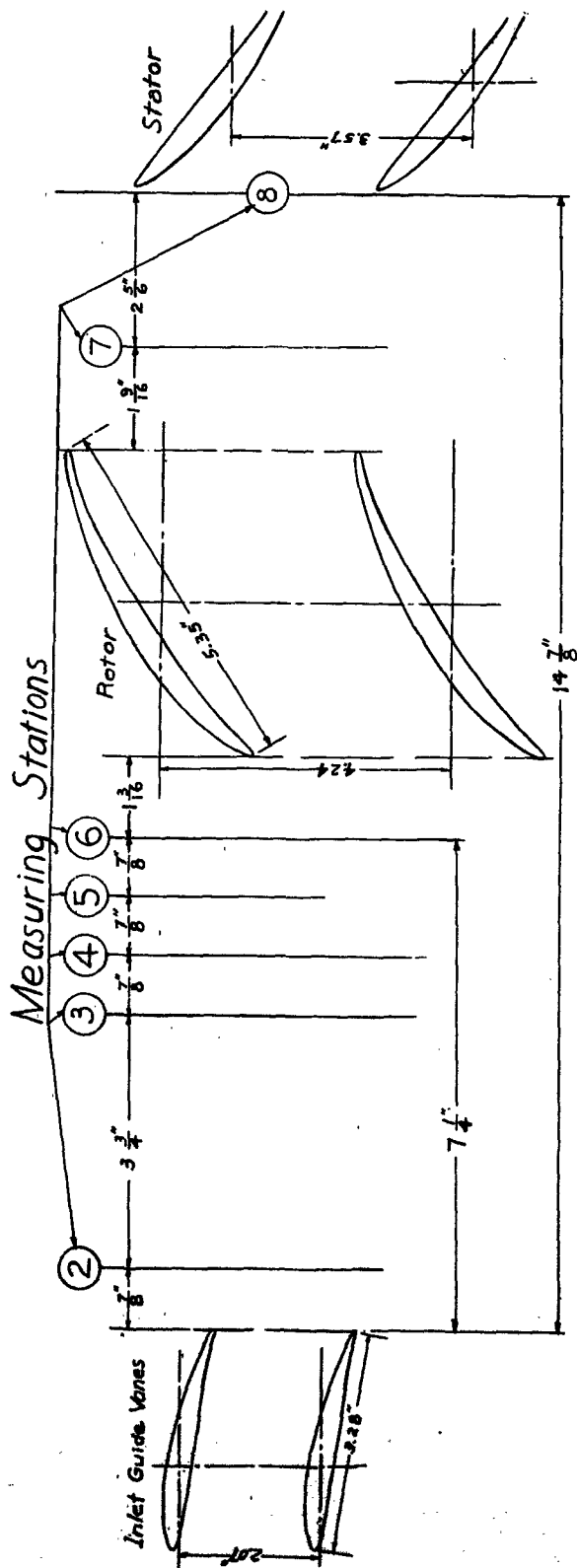
Figure 4. Geometry of Blades & Distances of Measuring Stations
At Survey Radius
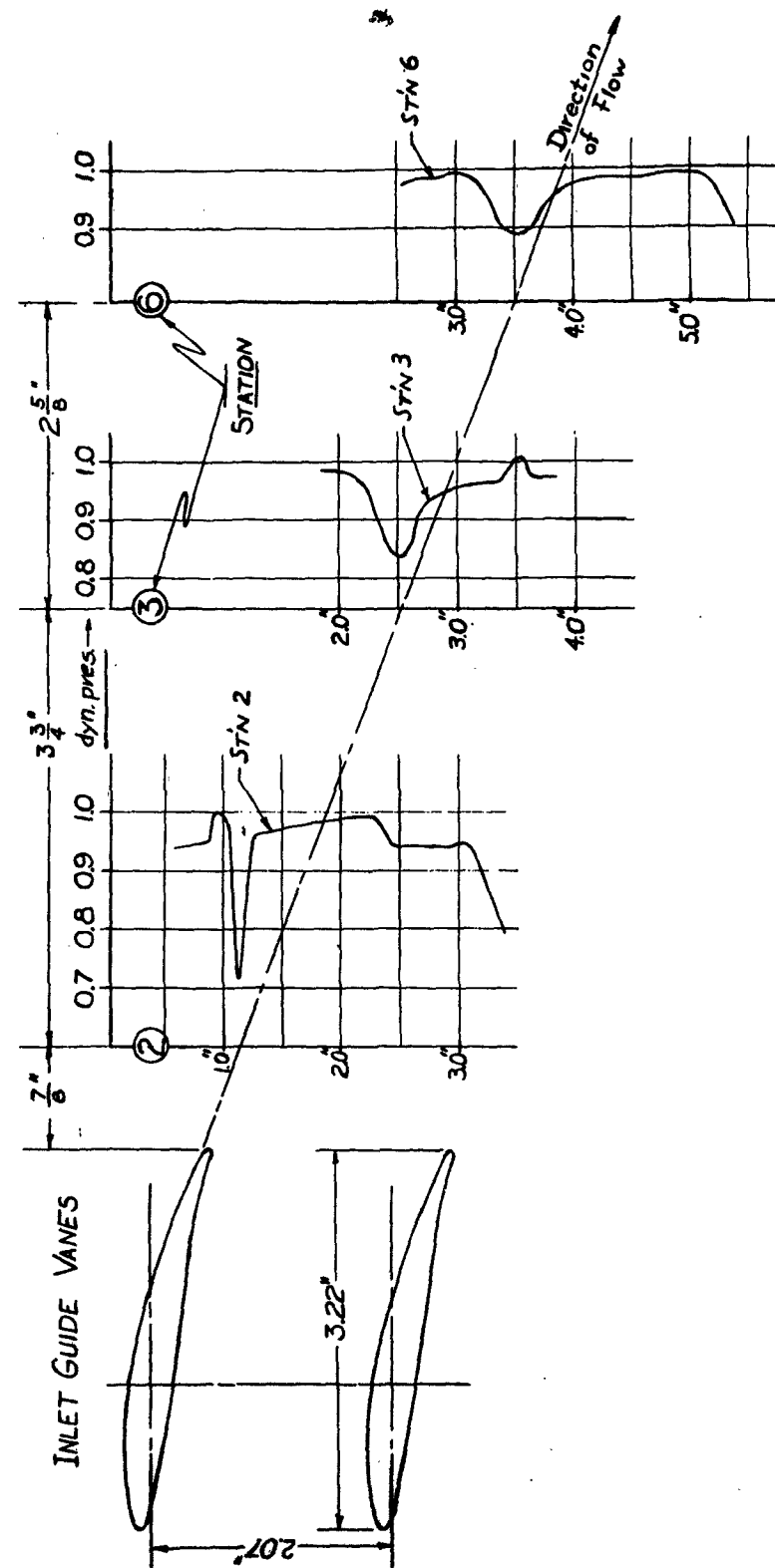
Fig. 5   Dynamic Pressure Distribution-$\left[\frac{dyn.pres.}{(dyn.pres.)@\textcircled{2}_{max}}\right]$
of Wake behind Inlet Guide Vanes

Case 1   Before Inlet Guide Vanes, Fluctuation Intensity = 0.24%

Case 2a   Between Inlet Guide Vanes and Rotor, Fluctuation Intensity = 6.13%

Case 2b   Between Inlet Guide Vanes and Rotor, Fluctuation Intensity = 0.39%

Fig. 6
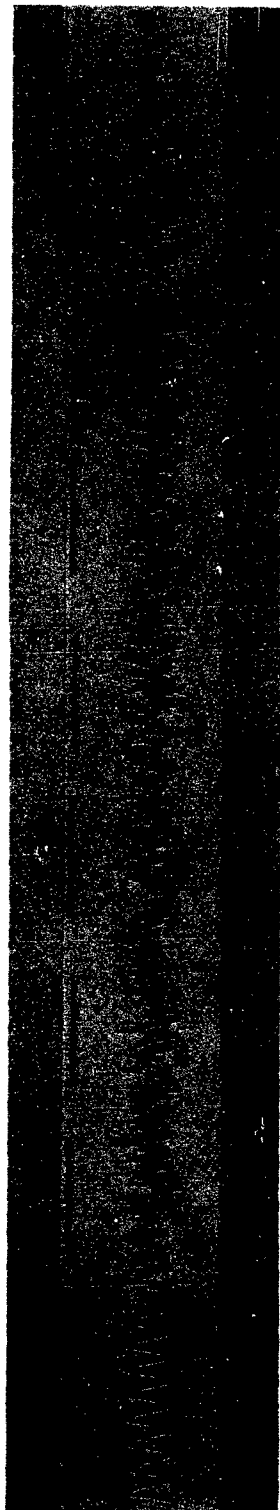
Case 3a   Between Inlet Guide Vanes and Rotor, Fluctuation Intensity = 3.24%
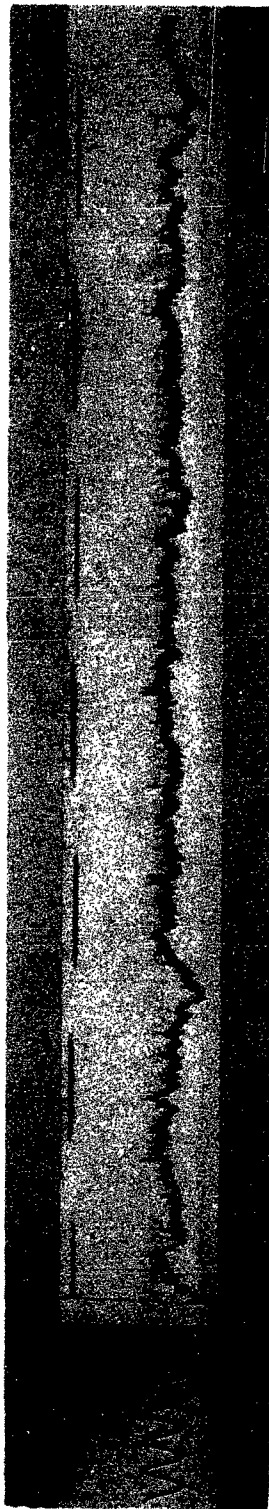
Case 3b   Between Inlet Guide Vanes and Rotor, Fluctuation Intensity = 0.35%

Fig. 7
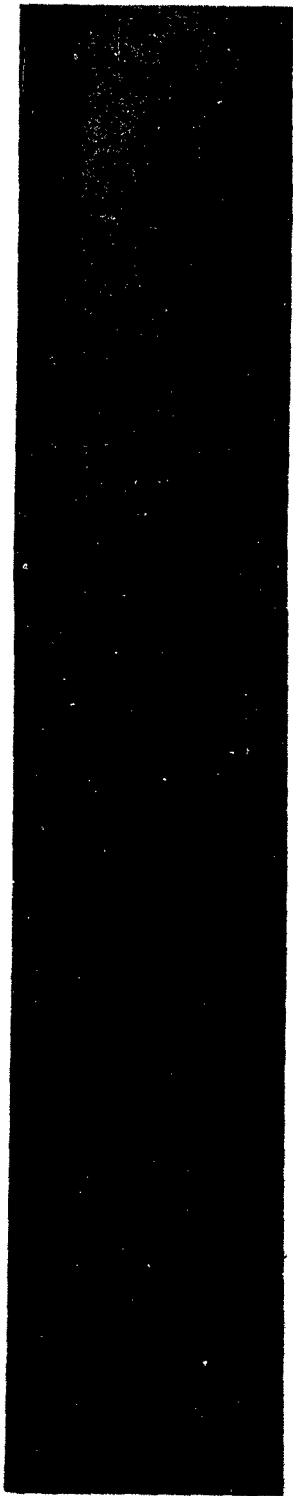
Case 5a   Between Inlet Guide Vanes and Rotor, Fluctuation Intensity = 2.84%

Case 5b   Between Inlet Guide Vanes and Rotor, Fluctuation Intensity = 0.45%

Fig. 8
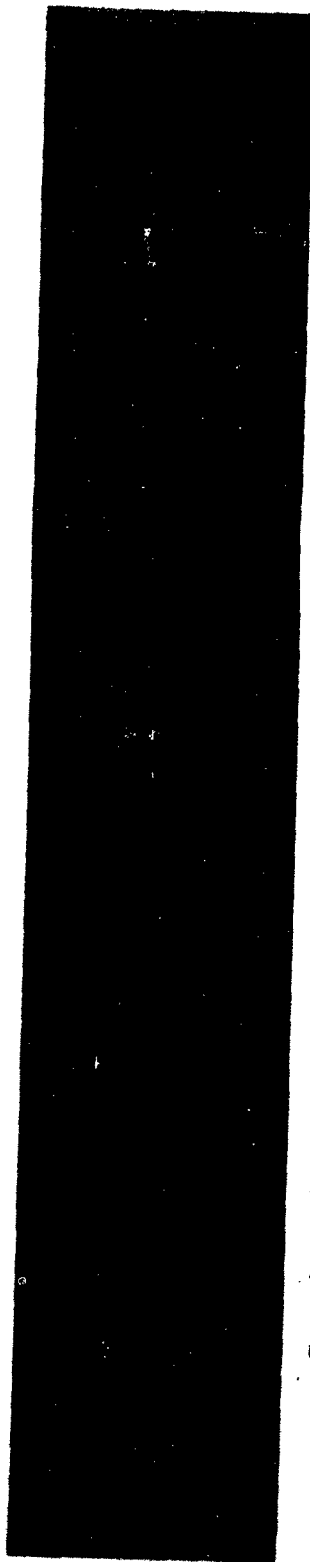
Case 6a   Between Inlet Guide Vanes and Rotor, Fluctuation Intensity = 2.93%
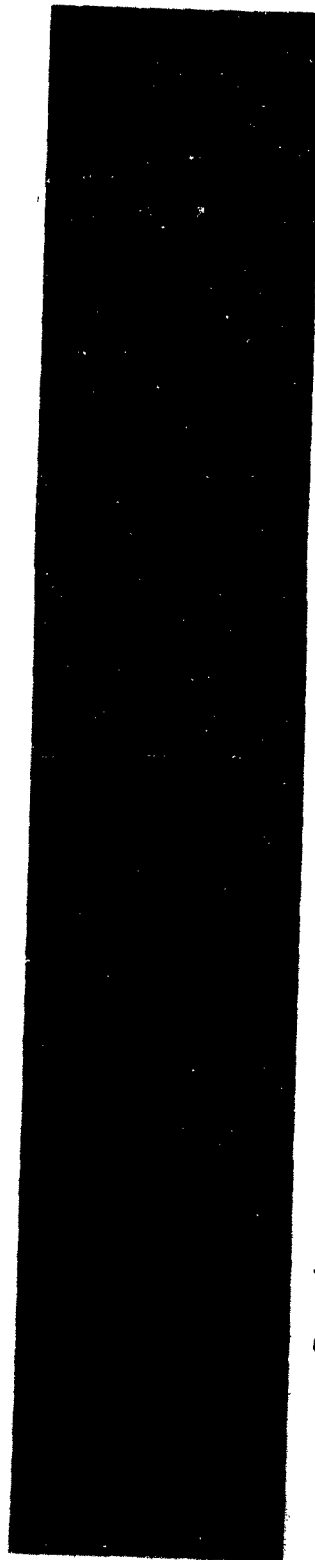
Case 6b   Between Inlet Guide Vanes and Rotor, Fluctuation Intensity = 1.45%

Fig. 9
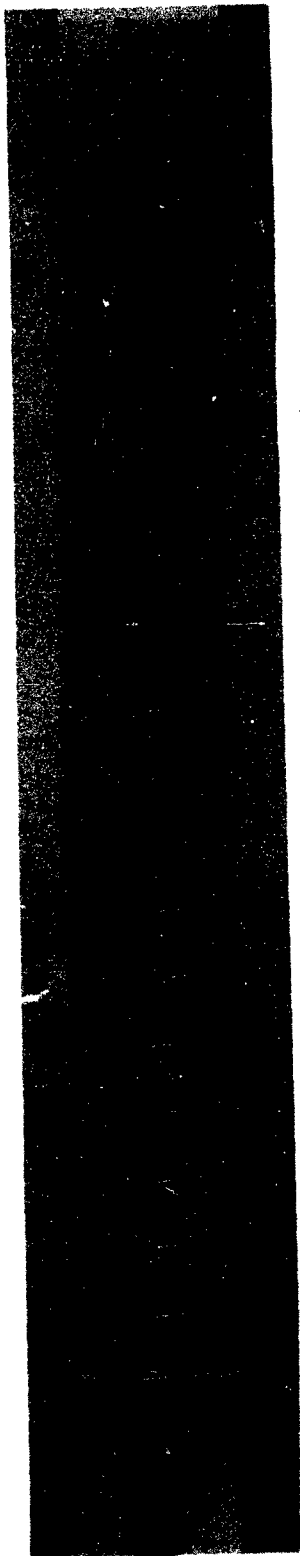
Case 7a   Between Rotor and Stator, Fluctuation Intensity = 5.47%
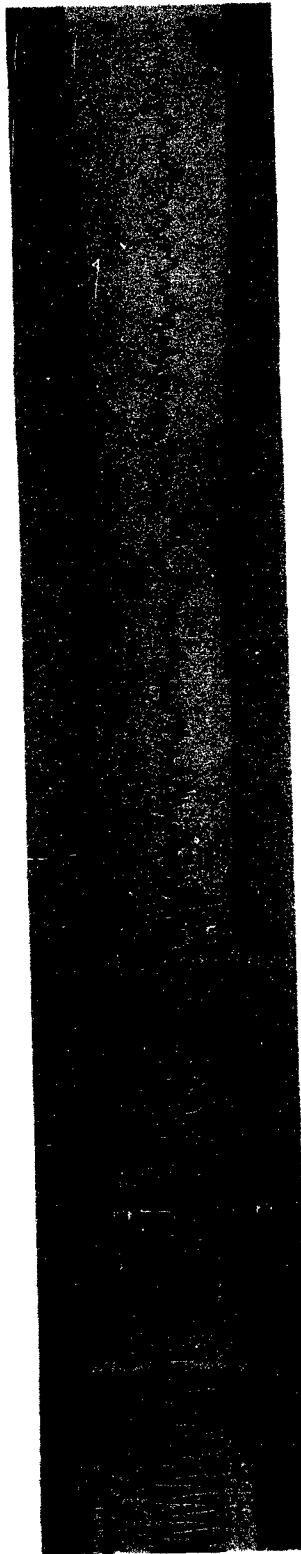
Case 7b   Between Rotor and Stator, Fluctuation Intensity = 2.20%

Fig. 10

Case 8   Between Rotor and Stator, Fluctuation Intensity = 3.16%

Case 9   Behind Stator, Fluctuation Intensity = 1.3%
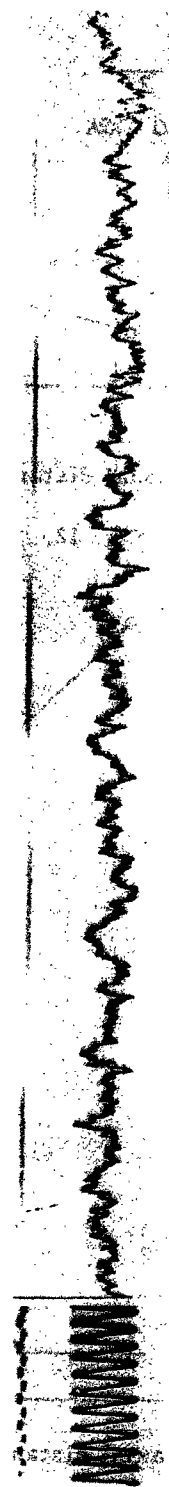
Case 10   Behind Stator, Fluctuation Intensity = 1 32%

Fig. 11
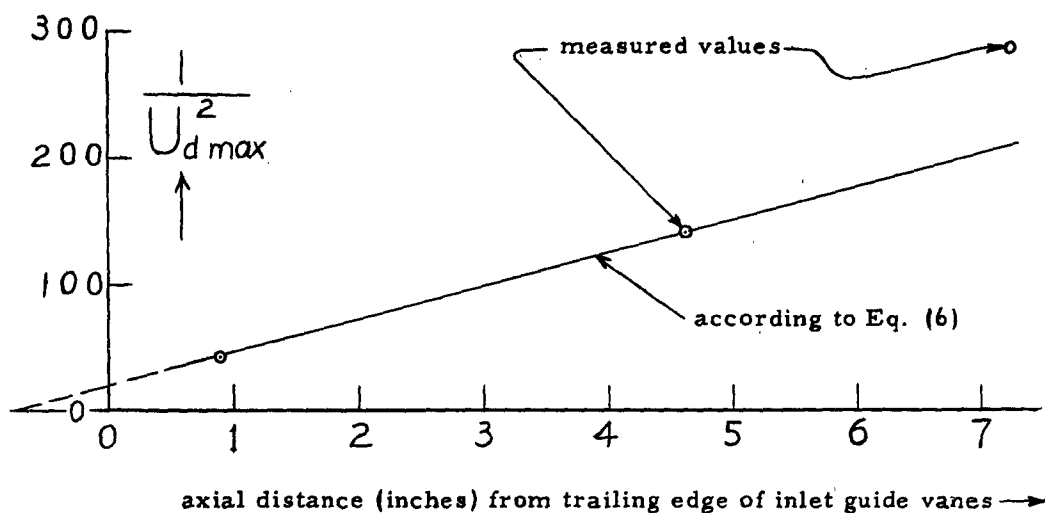
Fig. 12.   DECAY OF WAKE BEHIND INLET GUIDE VANES
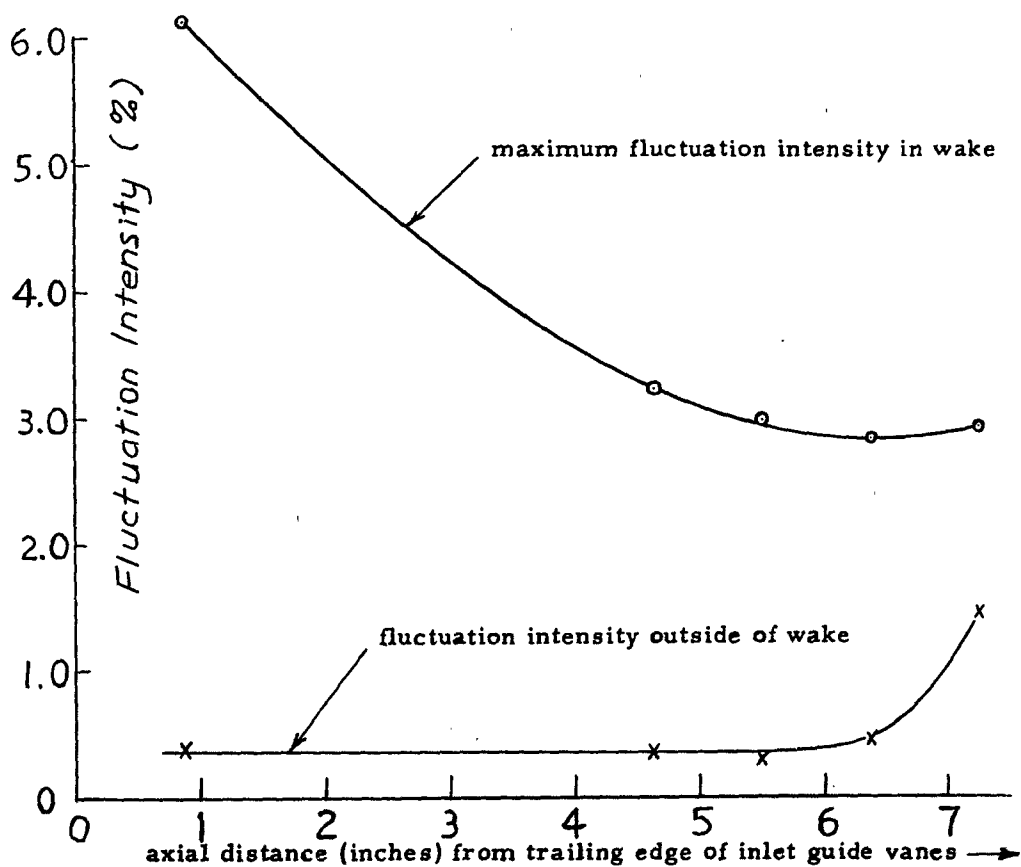
Fig. 13.   FLUCTUATION INTENSITY BEHIND INLET
GUIDE VANES
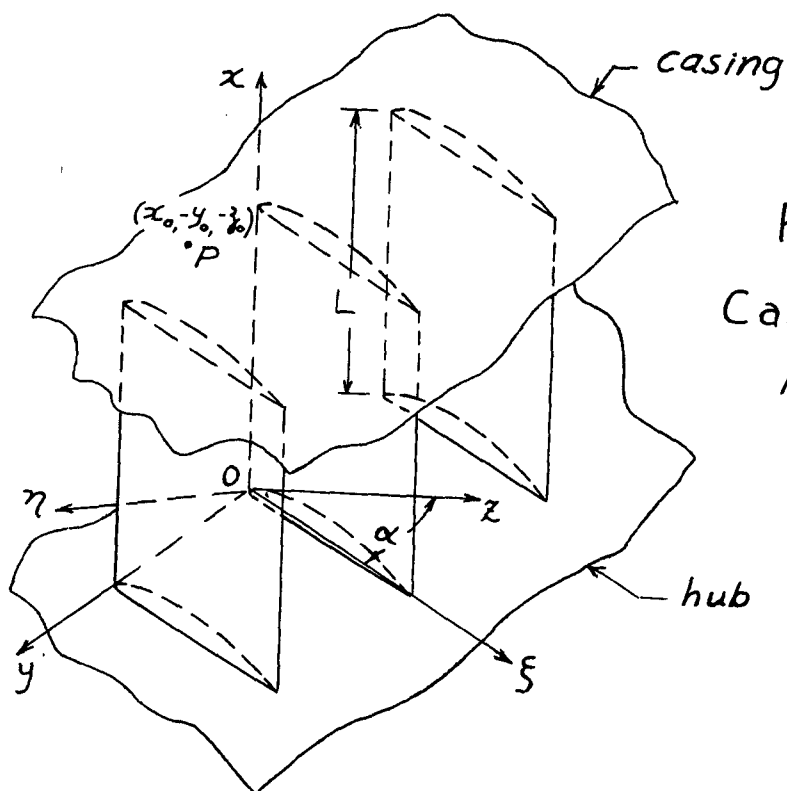
Fig 14
Cascade of Airfoils
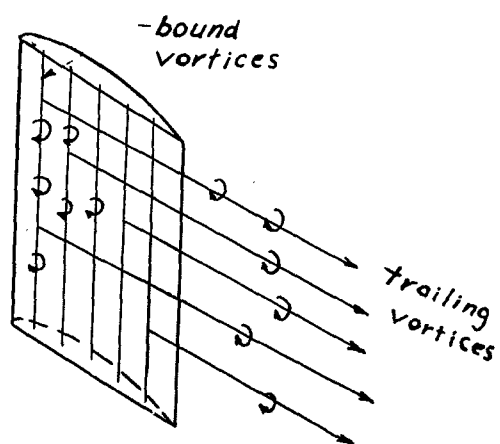
Fig. 15
Bound and Trailing Vortices
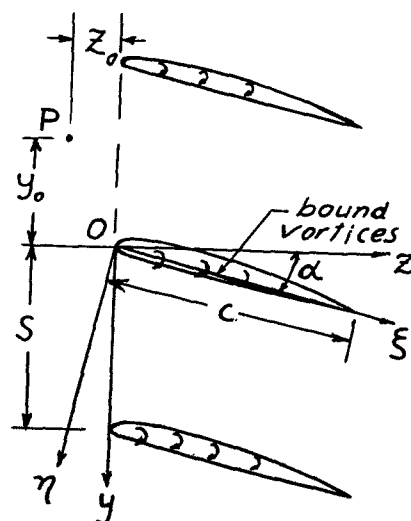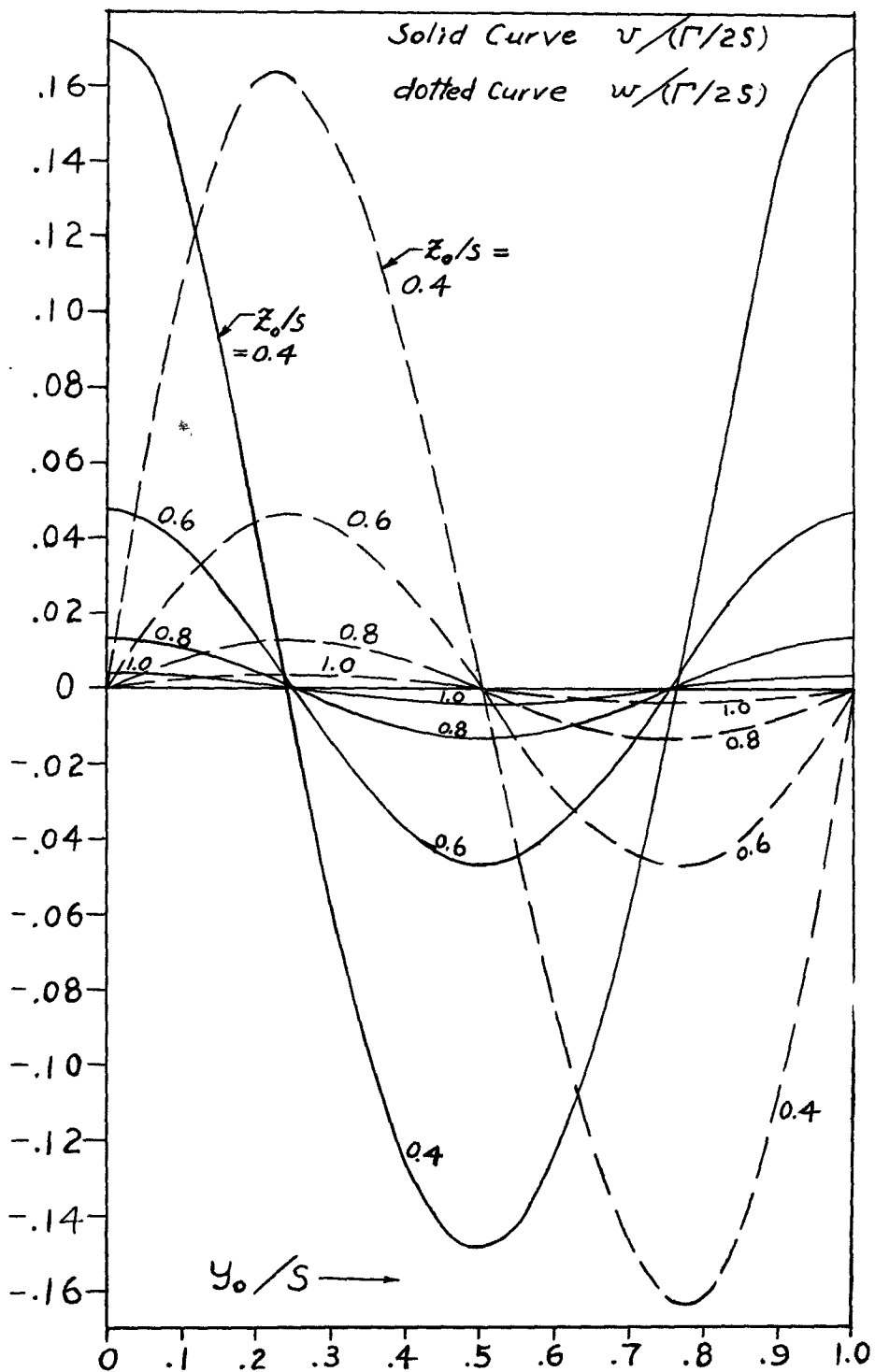

Fig. 16
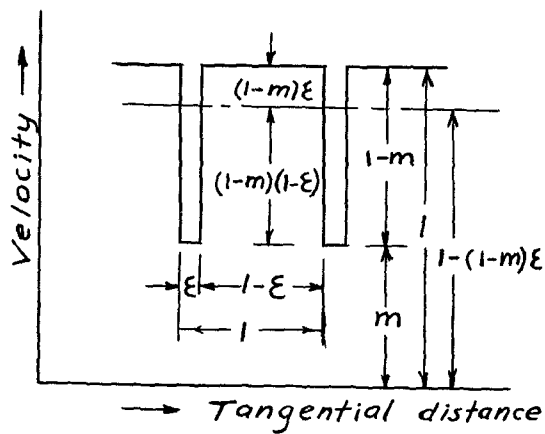Cascade Scheme
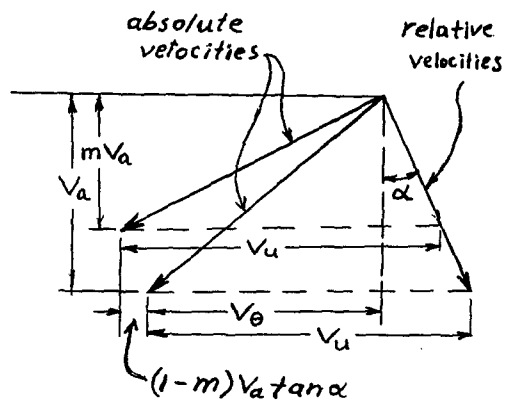
Fig. 17. Induced Velocity due to Cascade of vortices

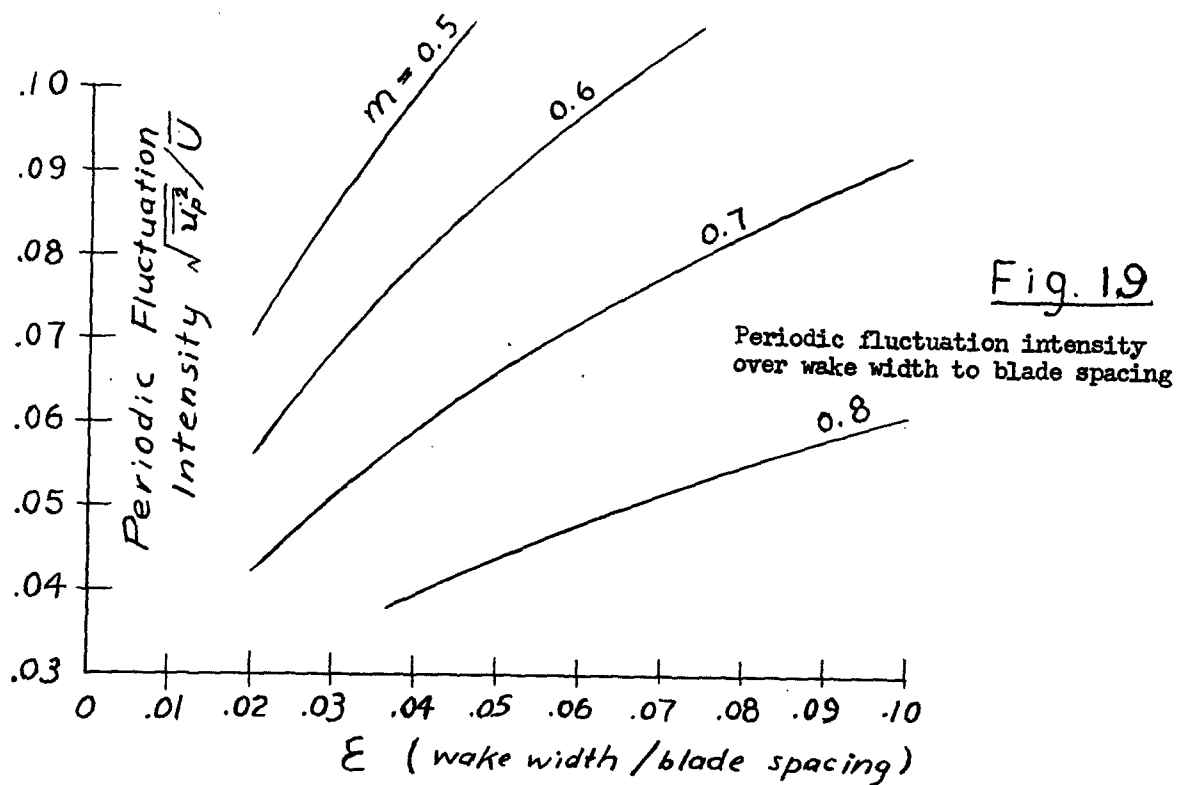Fig. 18
Wake Scheme

Fig. 20
Velocity Scheme

Fig. 19

Periodic fluctuation intensity
over wake width to blade spacing